Combined electrical and resonant optical excitation characterization of multi-quantum well InGaN-based light-emitting diodes

Cite as: AIP Advances **6**, 075108 (2016); https://doi.org/10.1063/1.4959100
Submitted: 02 June 2016 . Accepted: 06 July 2016 . Published Online: 14 July 2016

S. Presa, P. P. Maaskant, M. J. Kappers, C. J. Humphreys, and B. Corbett

Combined electrical and resonant optical excitation characterization of multi-quantum well InGaN-based light-emitting diodes

S. Presa,[1,2,a] P. P. Maaskant,[1] M. J. Kappers,[3] C. J. Humphreys,[3] and B. Corbett[1]
[1]*Tyndall National Institute, University College Cork, Lee Maltings, Dyke Parade, Cork, Ireland*
[2]*School of Engineering, University College Cork, Cork, Ireland*
[3]*Dep. Material Science and Metallurgy, University of Cambridge, CB3 0FS, Cambridge, United Kingdom*

(Received 2 June 2016; accepted 6 July 2016; published online 14 July 2016)

We present a comprehensive study of the emission spectra and electrical characteristics of InGaN/GaN multi-quantum well light-emitting diode (LED) structures under resonant optical pumping and varying electrical bias. A 5 quantum well LED with a thin well (1.5 nm) and a relatively thick barrier (6.6 nm) shows strong bias-dependent properties in the emission spectra, poor photovoltaic carrier escape under forward bias and an increase in effective resistance when compared with a 10 quantum well LED with a thin (4 nm) barrier. These properties are due to a strong piezoelectric field in the well and associated reduced field in the thicker barrier. We compare the voltage ideality factors for the LEDs under electrical injection, light emission with current, photovoltaic mode (PV) and photoluminescence (PL) emission. The PV and PL methods provide similar values for the ideality which are lower than for the resistance-limited electrical method. Under optical pumping the presence of an n-type InGaN underlayer in a commercial LED sample is shown to act as a second photovoltaic source reducing the photovoltage and the extracted ideality factor to less than 1. The use of photovoltaic measurements together with bias-dependent spectrally resolved luminescence is a powerful method to provide valuable insights into the dynamics of GaN LEDs. [http://dx.doi.org/10.1063/1.4959100]

I. INTRODUCTION

InGaN-based light-emitting diodes (LEDs) have reached wall-plug efficiencies in excess of 80%[1] making these devices strong candidates for general illumination. Nevertheless, there are several challenges still to overcome such as the sub-linear increase of the light output at high current densities, known as 'droop'[2–4] and the lack of efficient devices with wavelengths in the 530 nm – 630 nm range, known as the 'green gap'.[5,6] Addressing these challenges requires unambiguous identification of the different underlying mechanisms of current transport and recombination in LEDs which are grown under different conditions and can result in varying alloy fluctuations, interface qualities and doping profiles for nominally identical structures. Thus effective characterization methods are required to study the devices.

In this paper, we have used resonant optical pumping of the InGaN/GaN multi-quantum well (MQW) region on operational LEDs under different pump powers and bias conditions and measured the emission spectra and current – voltage characteristics. This allows the study of varying the carrier generation on the device characteristics: Electrical forward biasing of an LED moves holes and

[a]silvino.presa@tyndall.ie

electrons from the p and n-sides of the junction respectively which enter the MQWs and recombine. The electron and hole densities in the individual quantum wells (QWs) will not necessarily be uniform.[7] In the case of resonant optical excitation of the QWs, the carrier generation is uniform but they re-distribute via voltage dependent transport and recombination processes. The effect of the polarization field in the QWs on the properties of LEDs has been well analyzed in several studies[8,9] as has the effect of varying the relative thickness of the wells and barriers.[10] Here we characterize two LED structures with 5x and 10x 1.5 nm thick QWs and quantum barriers (QBs) of 6.6 nm & 4 nm respectively, along with a commercial wafer material. The decrease of the QB thickness in the 10QW sample increases the polarization field in the barrier and reduces the field in the QW. On the other hand, the 5QW has a stronger field in the QW and a weaker field in the thicker QB which results in a number of distinct electrical and optical properties. To further characterize the device we have measured the photovoltaic response which allows the comparison of the diode voltage ideality for different current and light output measurements. An extracted ideality >1 using light emission methods confirms a significant contribution of non-radiative recombination in the 5QW and 10QW samples.

The paper is organized as follows: section II describes the materials used and the LED devices fabricated. In section III we present the current-voltage and spectral characteristics of these devices under combined electrical and optical excitation. In section IV we extract diode ideality factors under different excitation and measurement conditions. We summarize and conclude in section V.

II. MATERIALS AND DEVICES

Two LED structures were grown by metal-organic chemical vapor phase deposition (MOCVD) on double-side polished low defect density templates from the same batch. These templates consist of a (0001) sapphire substrate followed by 3 μm of un-doped GaN and 1 μm of Si-doped n-GaN. The 5QW structure consisted of 5x 1.5 nm thick $In_{0.23}Ga_{0.77}N$ QWs with 6.6 nm thick GaN QBs. The 10QW structure consisted of 10x 1.5 nm thick $In_{0.23}Ga_{0.77}N$ QWs with 4 nm QBs. The QWs were grown using the quasi two-temperature (Q2T) method[11] where the InGaN QWs are grown at a temperature of 750°C and the first few nanometers of the GaN barriers are grown at the same temperature. The temperature was then ramped to 900°C to grow the remainder of the barrier. The 5QW (10QW) sample was capped with 110 nm (100 nm) of Mg-doped p-GaN. No electron blocking layer (EBL) or additional layers were grown. The actual thickness of these layers was confirmed using X-Ray diffraction. The wafers were grown in sequential runs with similar growth conditions. The expected emission wavelength of 470 nm was confirmed by photoluminescence (PL) measurements with full width at half maximum (FWHM) of around 25 nm. In addition to these samples we include a commercially sourced wafer from E Wave Corporation of unknown structure with similar wavelength emission around 465 nm to serve as a reference. The structure could be expected to contain an EBL and we measured the presence of a low In content InGaN layer under the QWs.

Substrate-emitting LEDs were formed by depositing 40 nm of Pd as an ohmic contact to the p-GaN in the form of disks with 100 μm diameter. Circular transmission length measurements (c-TLM) patterns were used to measure the contact properties.[12] Pd forms an ohmic contact as-deposited so no annealing was required.[13] The measured contact resistivity was $\sim 10^{-3}$ Ω·cm^2 for all samples while the sheet resistance of the p-GaN layer was 370 kΩ/sq, 430 kΩ/sq and 200 kΩ/sq for the 5QW, 10QW and commercial sample, respectively. Mesas of 120 μm diameter were formed by dry etching using BCl_3 chemistry. Non-alloyed Ti/Al/Ti/Au (20/170/5/250 nm) was deposited on the exposed n-doped GaN as a common (ohmic) n-contact.

III. CURRENT DENSITY – VOLTAGE AND PIEZOELECTRIC FIELDS

Figure 1(a) shows the forward current density versus voltage (J-V) characteristics of diodes from each sample on a semi-logarithmic scale. All show an underlying diode characteristic $J = J_0 \exp(q\,(V - IR_s)\,/n_{elec}kT)$ where J_0 is the saturation current density, q the electron charge, R_s

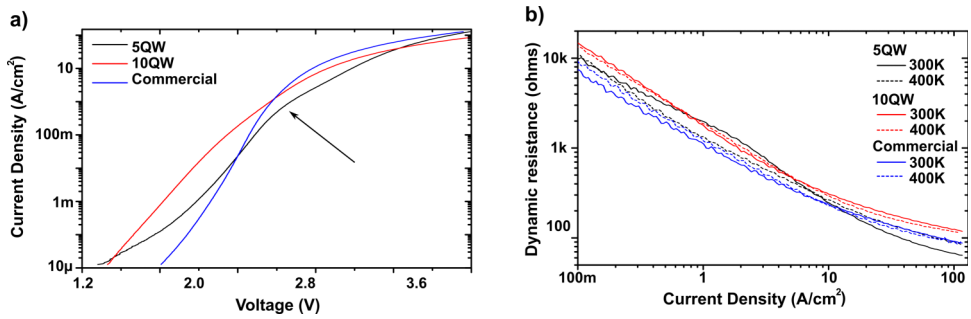

FIG. 1. a) Semi-log scale current density - voltage (J-V) curve at 300 K illustrating the different exponential rise of current for each sample. The arrow highlights a change in character of the 5QW sample. b) Semi-log scale dynamic resistance versus current at 300 K (continuous lines) and at 400 K (dotted lines).

the series resistance of the diode, n_{elec} the electrical ideality factor, k the Boltzmann constant and T the absolute temperature. For V < 2.5 V there is an exponential rise in the current before additional voltage is dropped across resistive parts in the diode. The 5QW draws a factor of 10 less current for the same voltage when compared with the 10QW during the exponential rise (2.0 V to 2.5 V) despite having a thinner active region. The commercial sample draws least current below 2.5 V and more current above 2.8 V with a larger slope of the log J - V curve indicating a lower n_{elec}. The ideality factor gives an insight about the underlying transport and recombination processes and is discussed later. The 5QW sample has a distinct decrease in the slope of the log J-V curve at around 2.6 V which is not present in devices from the other two samples. We plot the dynamic resistance, R_{dyn}, of the devices in Fig. 1(b) as a function of J at 300 K and 400 K. We note the distinct shape of R_{dyn} for the 5QW sample at 300 K (black continuous line in the plot) with a change in the rate of decrease at around 2 A/cm^2. This distinct resistance change does not show when the sample is heated to 400 K (dotted black line).

A difference in the thickness of the barriers impacts the balance of the piezoelectric fields between the quantum wells and barriers. The distribution of the voltage in a p-i (MQW)-n structure with a built-in voltage V_{bi} and applied voltage V results in a relation between the piezoelectric fields in the QW (E_w) and QB (E_b) as:[10,14,15]

$$NE_wL_w + (N+1)E_bL_b = V - V_{bi} \tag{1a}$$

or

$$E_w = (V - V_{bi})/NL_w - (N+1)E_bL_b/NL_w \tag{1b}$$

where L_w is the thickness of each QW, L_b the thickness of the QB, and N is the number of QWs.

The fields in the QWs are opposite to those in the QBs. The field in the QW is 12% greater for the 5QW sample compared with the 10QW sample. The consequent weaker field in the QB of the 5QW sample together with its greater L_b results in an overall combined confinement potential due to both the well and barrier (Fig. 2(a)) which can lead to a greater confinement of carriers, especially holes. As V is increased towards V_{bi} the field across the barrier reduces further while additional carriers are injected. Figure 2(b) shows the field profile for the 5QW at 2.6 V where up to four electron states are calculated which can lead to carrier trapping. Similar effects are calculated for the hole states. At higher temperatures the thermal energy allows carriers to escape this potential.

To gain further insight, we measure the emission spectra under electrical excitation and under combined electrical and resonant optical pumping with the setup sketched in Fig. 3. Figure 4 shows the spectral emission under pure electrical and under combined optical and electrical excitation. The normalized spectra under electrical excitation from 2.6 V to 3.0 V with a step of 0.1 V are shown in the left column with the plots belonging to the 5QW, 10QW and commercial sample from top to bottom respectively. The spectra are modulated by the Fabry-Perot resonances due to the reflection from the GaN to sapphire interface. The right column in Fig. 4 shows the spectra with combined optical excitation. Here the LEDs were illuminated through the polished substrate

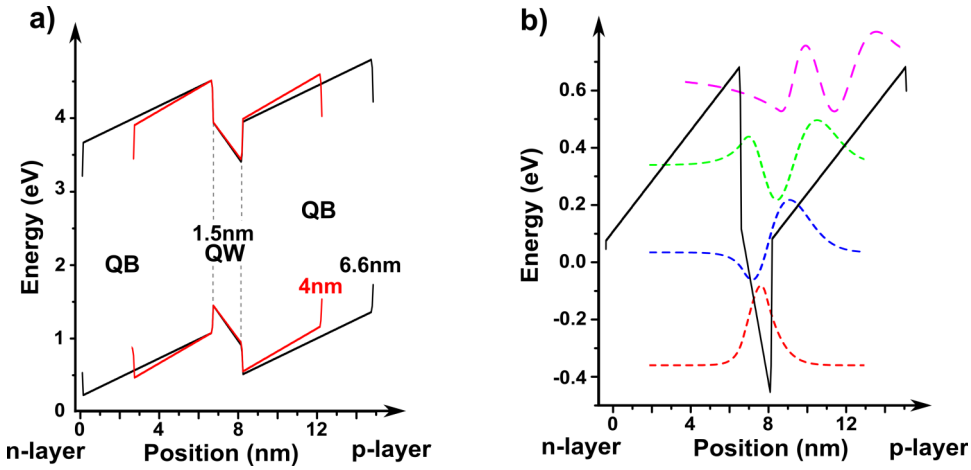

FIG. 2. a) Unbiased conduction and valence bands of the 5QW and 10QW structures with 6.6 nm thick (black) and 4 nm thick QBs (red) calculated using SiLENSe from STR Ltd. b) Simulated conduction band diagram and confined electron wavefunctions at a forward bias of 2.6 V for the 5QW (6.6 nm thick QBs) structure.

using a 405 nm laser diode with a maximum light power output of 20 mW as the excitation source. There is a double pass of the light from the partially reflective contact. The use of 405 nm assures that absorption is only in the QWs leading to uniform pumping of the QWs. These spectra were measured under an optical excitation of 200 W/cm^2 with an applied bias from -1.5 V to +1.5 V and a step of 0.5 V.

At low currents the polarization field in the QWs is enhanced because, under forward bias, the external electric field is in the same direction as the field in the QWs (Eq. (1b)). The increased field results in a red shift of the emission wavelength. At higher currents, the effect of the field can be screened by the increase in the carrier density in the QWs. This screening translates into a blue shift in the emission spectra. Figure 4(a) shows little variation in the spectra from the 5QW

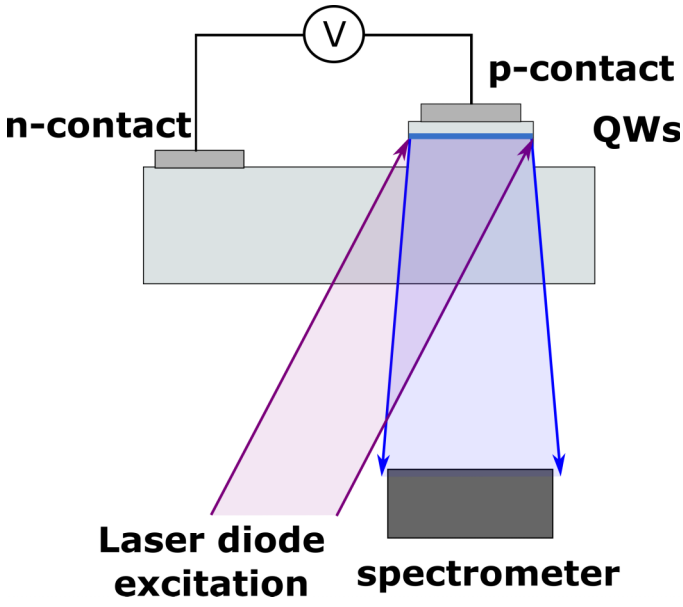

FIG. 3. Schematic view of the optical resonant excitation set up for bias-dependent PL. The laser is directed at approximately 30° to the surface normal through the polished substrate and excites only the QWs. A spectrometer collects light emitted perpendicular to the device.

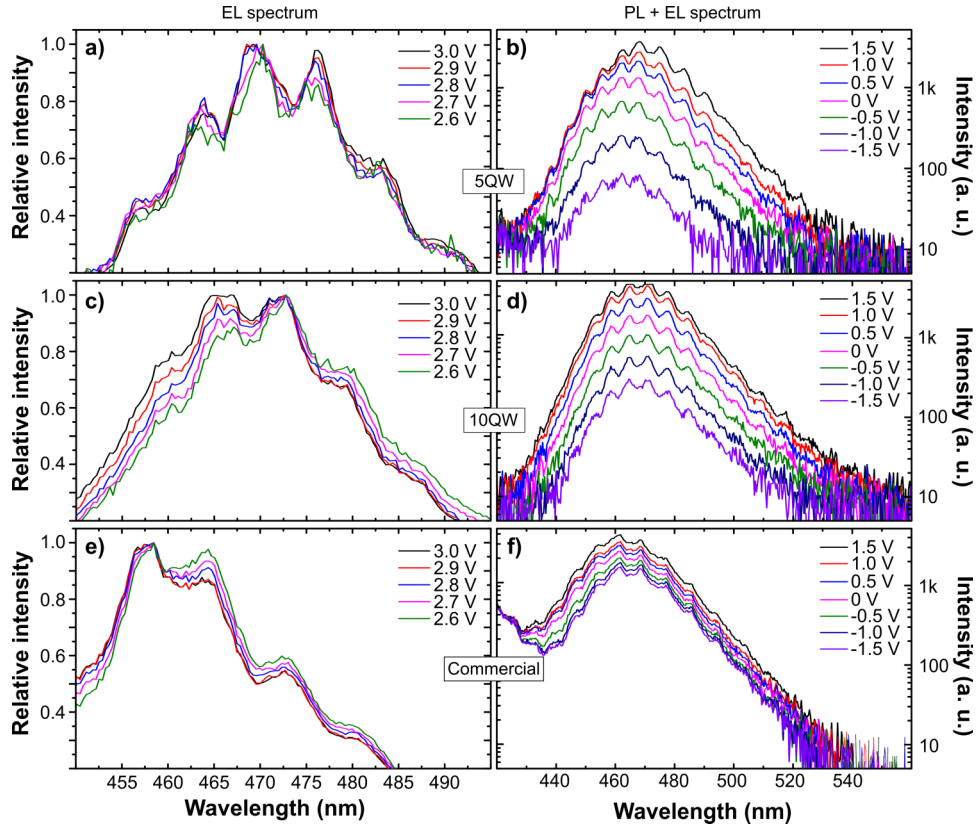

FIG. 4. Left column: Electroluminescence spectra for the a) 5QW, c) 10QW and e) commercial samples with an applied voltage from 2.6 V to 3.0 V. Right column: Emission spectra with combined resonance excitation (200 W/cm^2) while varying the voltage applied from -1.5V to +1.5 V in forward bias for the b) 5QW, d) 10QW and f) commercial sample.

sample under increased electrical bias for the selected voltage range. This indicates an equilibrium between change of the polarization fields and the increase in the carrier density. This is in contrast to the 10QW and commercial samples which both show a relative increase in the intensity within the Fabry-Perot resonances at shorter wavelengths with increasing voltage (Fig. 4(c), 4(e)). Thus, the increase in carrier density for both these samples is dominant over an increase of the field in the wells.

Under combined electrical and optical excitation the 5QW sample is distinguished by a strong suppression in the emission at longer wavelengths with reducing the electrical bias (Fig. 4(b)). In addition, there is a reduction in intensity and FWHM. Emission at longer wavelengths originates from the electrons at the bottom of the QWs and the well is deepened (reduced in energy) in forward bias as the bias field is in the same direction as the piezoelectric field in the well. Therefore, a reduction in the external field in forward bias will affect mainly the emission at longer wavelengths. Under reverse bias the external field helps carriers to escape from the QWs reducing the carrier density, which results in the reduced emission intensity for all wavelengths.

The spectra from the 10QW sample under the same conditions (Fig. 4(d)) do not show any significant difference between the longer and shorter wavelength part of the spectra and the decrease of the intensity is due to the reduction of the carrier density. Under optical excitation the commercial sample shows an additional emission peak at 420 nm (Fig. 4(f)) which is not affected by changes in the applied bias (not shown here). We believe that this is due to an n-doped InGaN layer (or superlattice) below the QW structure which is used in many commercial LEDs to improve the overall efficiency.[17] The absorption of the pump light by the InGaN underlayer provides an additional source of carriers (minority carrier holes) for the QWs which explains why, as the electrical bias is reduced, the reduction in the MQW emission intensity is much less than for the 5QW and 10QW

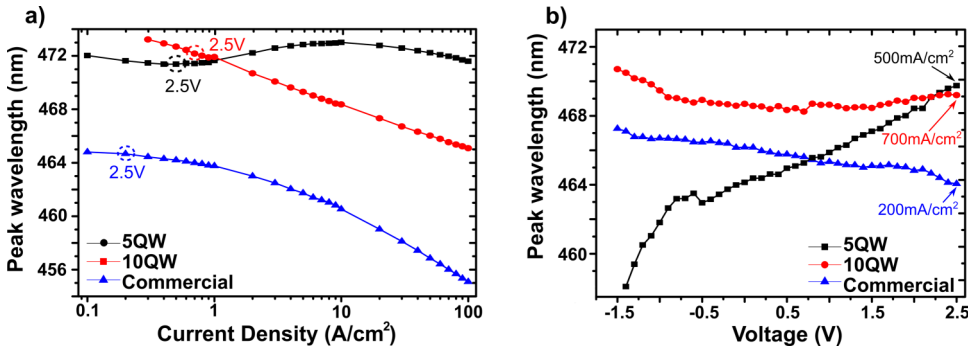

FIG. 5. a) Peak wavelength versus current under electrical excitation, b) peak wavelength versus voltage under optical (200 W/cm^2) and electrical excitation.

samples. We note that there is a significant amount light emission for all samples, and especially the commercial one, at short circuit (V = 0 V). This indicates that not all the photogenerated carriers escape at this condition.

The peak emission wavelength from these measurements is obtained by fitting a Gaussian function to the spectra. Figure 5(a) shows the peak wavelength with current under electrical excitation alone while Fig. 5(b) shows the peak wavelength with applied bias and optical excitation of 200 W/cm^2. These plots highlight the distinctive properties of the 5QW sample: At very low current there is a slight blue shift due to the band-tail states of the QWs being filled with carriers before a red shift is measured. At high currents the effect of the piezoelectric field is screened and there is a blue shift again. This is in line with the larger polarization field in the QW of the 5QW sample. The 10QW and commercial samples show only a blue shift of the peak wavelength with increasing current indicating that the emission is dominated by the screening of the piezoelectric field by filling of the states in the QW.

Figure 5(b) shows that the change in the direction of the electric field (voltage bias) from opposite to the same direction of the piezoelectric field in the QWs causes a large red-shift in peak wavelength for the 5QW sample. This is also in agreement with the piezoelectric field being larger in this 5QW sample. The emission peak of the 10QW and commercial samples show a slight red-shift at high reverse bias where only a small amount of light is detected. This is due to the bottom of the QW starting to slope in the direction of the applied negative bias field. To help compare the plots from Fig. 4 and Fig. 5 the current density when 2.5 V is applied is indicated. The addition of the optical excitation shifts the emission peak to shorter wavelengths for all the devices which is explained by the increase in the carrier density in the wells under optical excitation.

5QW and 10QW samples with large contact area to allow measurement at low current densities, show broad yellow band (YB) emission (500 nm – 600 nm) under both low forward bias electrical injection and under optical pumping. When the devices are reverse biased and optically pumped the emission from the QW is extinguished at -3 V while the YB emission remains constant but proportional to the pump power.[30] The YB is not present if the MQW region is etched away and illuminated by 405 nm light. This suggests that the YB origin is in the MQW region. We believe it is associated with traps in the QB particularly with the low-temperature grown region. Carbon - oxygen complexes with defect levels 0.75 eV above the valence band maximum have been recently shown to be the source of yellow emission in undoped GaN.[18] Such defects on the upper side of each quantum well would promote hole tunneling and thus explain the higher ideality factors measured with these samples.

IV. IDEALITY FACTOR

The electromotive force (qV) which causes the separation of the quasi-Fermi levels (QFLs) for electrons and holes in the active region of an LED drives current transport and light emission with – to a first approximation - a Boltzmann dependence of $J, L \sim exp\,(qV/n_{ideal}kT)$ where n_{ideal} is

the ideality factor. It is tempting to extract the voltage dependent ideality factor $n_{ideal}(V)$ and use it to assign dominant underlying physical mechanisms for the transport or recombination at a given voltage. This is because the current due to diffusion in a p-n homojunction has an ideality of 1 whereas Shockley-Read-Hall (SRH) trap related recombination at the junction is maximized with an ideality of 2. Similarly, light emission L which depends on the product of the hole and electron densities, $p \times n$, results in $L \sim exp\left(qV/n_{light}kT\right)$. This can only be attempted if the voltage measured is the QFL separation which fails in the presence of non-ohmic contacts or if resistance effects are present. For an LED the QFL separation is less than the bandgap voltage (2.64 V here) as a higher QFL indicates gain. Even then, a GaN LED is composed of many hetero-interfaces, with inbuilt piezoelectric fields and a high density of defects making it difficult to assign the ideality unambiguously to a particular process. Reference 19 has shown that the electrical ideality is reduced if the QBs are intentionally doped. Transport of carriers by tunneling can have a strong influence on the ideality factor[20,21] and has been reported to lead to idealities which range from 3.5 up to 7.[22] However, we must distinguish between tunnel currents which result from carrier being transported directly across the junction as against tunnel currents which result in carriers entering the quantum wells. Nevertheless, a GaN homojunction p-n diode with near unity ideality has been recently demonstrated[23] while, with improving device quality, an InGaN LED with an electrical ideality factor of 1.1 has been shown.[24] The low ideality was revealed by minimizing the device resistance and was correlated with a better internal quantum efficiency in the LED.[24] Using current continuity an equivalent circuit for a GaN LED can be obtained.[25] The total current J, whether electrical or optically generated, can be presented as $J = J_{rad} + J_{nrad} + J_t + J_{leak} + J_{Auger}$ where J_{rad} is the radiative recombination current component, J_{nrad} is the non-radiative defect related recombination current, J_t is tunneling current through the junction, J_{leak} represents a carrier leakage current and J_{Auger} is the current component related to Auger recombination. The Auger and carrier leakage terms are not significant at the low current densities investigated here.

Here, we make four different measurements of the ideality using electrical and combined electro-optic techniques. We first extract the voltage dependence of the electrical ideality factor n_{elect} from the J-V measurements at 300 K (continuous lines) and 400 K (dotted lines) as shown in Fig. 6. At 300 K the ideality factors for the 5QW and 10QW samples are close to 3.5 in the 1.6 – 2.4 V range. Above 2.4 V the resistance associated with the small device area obscures the true ideality factor. These relatively high values suggests that a tunneling mechanism is involved in the current transport at 300 K. This also corresponds with the defect emission measured and the higher current drawn at these voltages compared with the commercial sample. For the commercial sample, n_{elect} is close to 2 which could be associated with the current transport or SRH recombination in the intrinsic region.

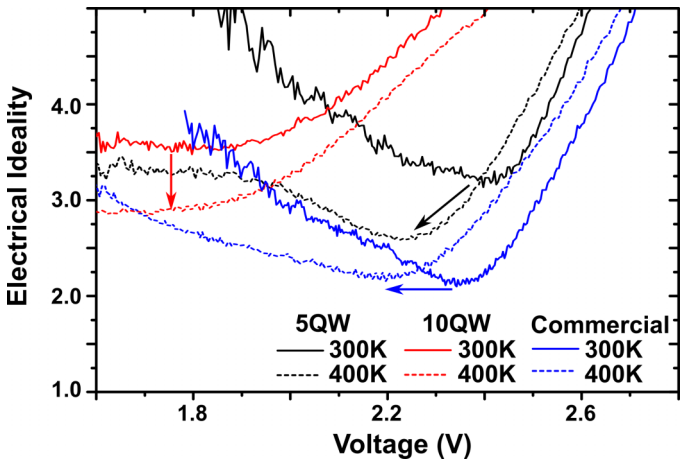

FIG. 6. Electrical ideality factors against voltage using J-V measurements at 300 K (continuous line) and 400 K (dotted lines). The ideality factor for the 5QW and 10QW are temperature dependent.

When the temperature is increased to 400 K, the minimum ideality factor of the 5QW is reduced to ~2.5 while the 10QW is reduced to ~2.8. The ideality factor of the commercial sample increases slightly from 2 and the voltage where the minimum occurs reduces by around 200 mV. A similar change happens with the 5QW and is due to the reduction of the bandgap with temperature.[26] We do not measure a change for the 10QW, though we cannot identify the position of the minimum ideality. The reduction in the ideality factor with the temperature is related to the contribution to carrier transport due to thermionic emission across the wells as the tunneling should be independent of temperature.

The light output can be approximated as $L = Bnp = Bn_i^2 exp\left(qV/n_{light}kT\right)$ where B is the radiative recombination coefficient, n_i the intrinsic carrier concentration and n_{light} is the ideality factor for the radiative recombination current. This ideality factor is extracted from the slope of the log L-V curve so measurement of partial output power from the LEDs is sufficient. We present the light output density (Luminescence/Area) versus voltage characteristics of the LEDs on a semi-logarithmic scale in Fig. 7. Similar levels of light are measured for both the 5QW and 10QW samples at a given voltage. As there is a larger current density driven by the 10QW sample at a given voltage (Fig. 1(a)) this indicates that there is greater non-radiative recombination in the 10QW device. The extracted values for n_{light} are plotted in the inset of Fig. 7 with minimum values of $\approx$ 1.5, 1.8 and 1.1 for the 5QW, 10QW and the commercial sample, respectively. An n_{light} of 1.1 as measured with the commercial sample is expected for radiative recombination with equal electron and hole densities. The origin of the higher n_{light} for the 5QW and 10QW is due to non-radiative recombination in the QWs. The ideality of the 5QW increases at a lower voltage than the 10QW. We should note that the 5QW and 10QW samples have no EBL to prevent carriers being injected at lower bias. The higher light emission intensity at V < 2.35 V for the 5QW and 10QW samples as compared to the commercial sample could be useful for some purposes despite its low efficiency.

Using the resonant optical pumping set up shown in Fig. 3 we measure the I-V characteristic from each sample from -4 V to +2.75 V under different illumination intensities. Figure 8 shows the characteristics where black lines indicate the measurement without any illumination (J_{dark}) and the coloured lines indicate the measurements with increasing the laser output power from 33 to 200 W/cm^2 with a step of 8.3 W/cm^2. Several observations can be made from these plots: At -4 V the 5QW and 10QW samples reach a saturation in the current collected indicating that all the photogenerated carriers in the QWs are extracted. While no quantum well emission is detected at this voltage, a weak yellow band emission is detected as discussed earlier. The measured photocurrent at reverse bias allows us to estimate the percentage of the light absorbed by these samples which is 5.6%, 12.5% for the 5QW, 10QW, respectively. This corresponds to absorption of 1.4% of the 405 nm light by each QW for the 5QW and 1.56% per QW for the 10QW sample. We should also note the effect of the partially reflective (60%) Pd contact, which allows a double pass of the light, which results in approximately 0.8-1% of the light from the laser being absorbed in each 1.5 nm

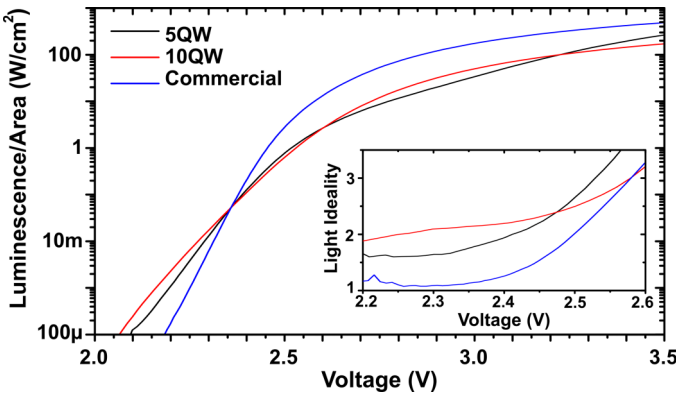

FIG. 7. Semi log scale light output density – voltage (L-V) at room temperature of the 5QW, 10QW and commercial sample. The sharper rise of the commercial sample (blue line) indicates lower ideality factor.

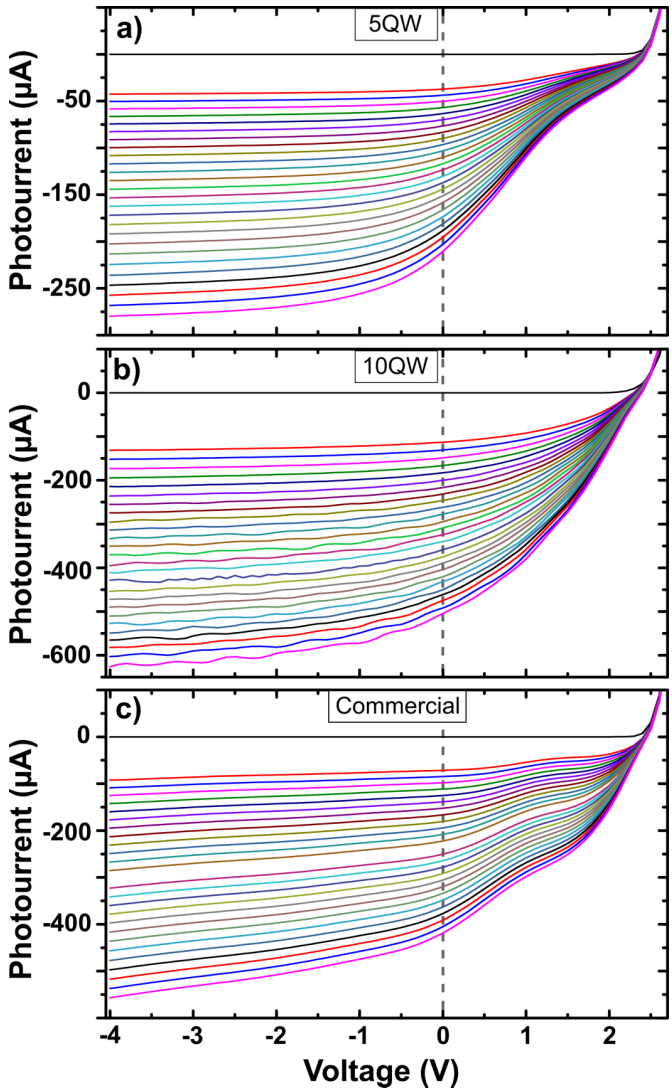

FIG. 8. Photoresponse measurements for a) 5QW, b) 10QW and c) Commercial sample. Black lines correspond to measurements without illumination while the coloured lines show the response with an increase in the optical excitation from 33 W/cm^2 to 200 W/cm^2.

thick QW per pass. For the commercial sample this analysis cannot be accurately performed due to additional absorption in the InGaN underlayer and the unknown number of wells.

These measurements show the effect of the thicker barriers of the 5QW sample as compared with the 10QW sample. At high reverse bias both samples have their QWs depleted with the ratio between their photocurrents being slightly higher than the factor of 2 that would be expected based on the number of QWs. Between 0 V and 2 V where the photovoltaic effect dominates we measure a strong voltage dependence in the extraction of the photogenerated carriers. In comparison with the 10QW sample the 5QW photocurrent produced for $V > 0$ reduces significantly. By measuring the luminescence from the samples as a function of voltage it is seen that the missing photocurrent is translated into a corresponding increase in light emission.[30] This shows that the carriers are being increasingly trapped in the overall QW/QB region of the 5QW sample at certain voltages due to the thicker barrier resulting in deeper confinement.[27] The reduction of the inbuilt field by the photovoltage confines the carriers even more increasing the carrier dwell time and allowing recombination processes to dominate. The reduced confinement in the 10QW sample on the other hand permits better escape of the carriers to higher voltages. A similar dependence of carrier escape on

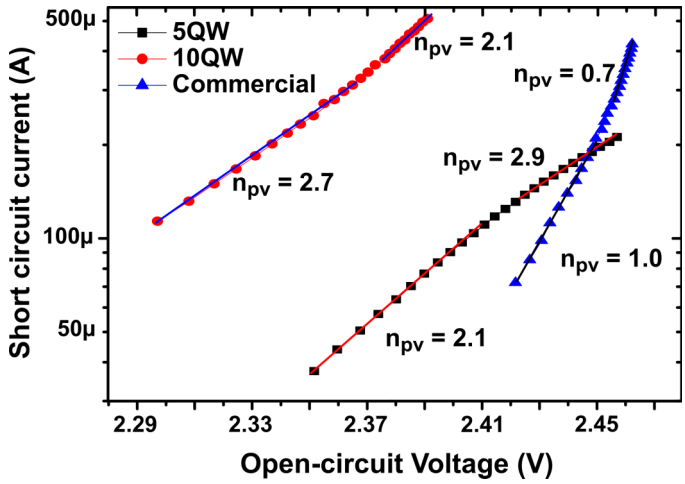

FIG. 9. Semi-log plots of short circuit photocurrent versus open-circuit voltage for the three samples along with the extracted ideality factors.

barrier thickness was reported in Ref. 28. The collected current in commercial sample does not fully saturate even at -4 V which is due to the depletion layer extending into the absorbing InGaN underlayer resulting in collection of holes which produce the small additional photocurrent. The carriers which remain in the QWs contribute to luminescence as seen in Fig. 4. The photocurrent of the commercial sample as with the 5QW sample shows a distinctive decrease around 1 V which results in a corresponding increase in photoluminescence. These measurements reveal differences in the properties of the diodes at voltages <2 V which are associated with trapping of carriers in the QWs.

The relationship between the short circuit current density J_{sc} and the open circuit voltage V_{OC} is given by $V_{OC} = [\frac{n_{pv}kT}{q}]ln(J_{sc}/J_0)$ allowing a photovoltaic ideality factor n_{pv} to be extracted from the measured log I_{sc}-V_{OC} curve. Figure 9 shows that this approximation holds for all samples despite the poor fill factor and the complex dynamics between these end points. Recall also from Fig. 4 that there is incomplete carrier escape at V = 0 V. The n_{pv} values give information about the recombination and transport mechanisms that take place in the intrinsic region without external contribution from the p- or n-side of the junction. In Fig. 9, the 5QW sample shows an increase in n_{pv} with voltage from 2.1 to 2.9 indicating a transition between processes and an increased non-radiative recombination. For the 10QW sample, n_{pv} is 2.7. This value is lower than n_{elec} but n_{pv} is measured at higher voltages. The commercial sample shows n_{pv} of 1 and less at higher voltages. We suggest this lower value comes about from the absorbing n-type InGaN layer as a second photovoltaic source in series which acts to reduce the measured voltage and effectively reduce the extracted ideality. The pump light absorbed in this underlayer can also re-emit at 420 nm and subsequently be absorbed in the MQW which will also contribute to increased photovoltaic performance. Auger recombination can lead to an electrically ideality of 2/3 but that is not the case here.

The fourth method to extract a voltage ideality factor is to measure the photoluminescence intensity under resonant optical pumping while keeping the external current to be zero.[29] This should be a more accurate method to measure the recombination ideality as it does not rely on the radiation to be represented by J_{sc} which is compromised by incomplete carrier extraction. With increased pump intensity, the PL increases exponentially with the generated V_{oc}. Figure 10 shows the measured data where the extracted ideality n_{pl} is indeed slightly lower than measured under the photovoltaic measurement. Again, the 5QW sample shows a change in the ideality around 2.4 V. The high values for n_{pl} show that non-radiative recombination in the quantum wells is a significant factor in the 5QW and 10QW sample. As with the PV measurement the commercial sample show $n_{pl} < 1$ which comes from diffusing holes created in the n-type InGaN recombining with electrons created in the MQW region enhancing the light emission at a given V_{oc}.

The diode ideality factors extracted under different electrical and optical excitation and summarized in table I, can be used to explain the recombination and transport properties of the devices.

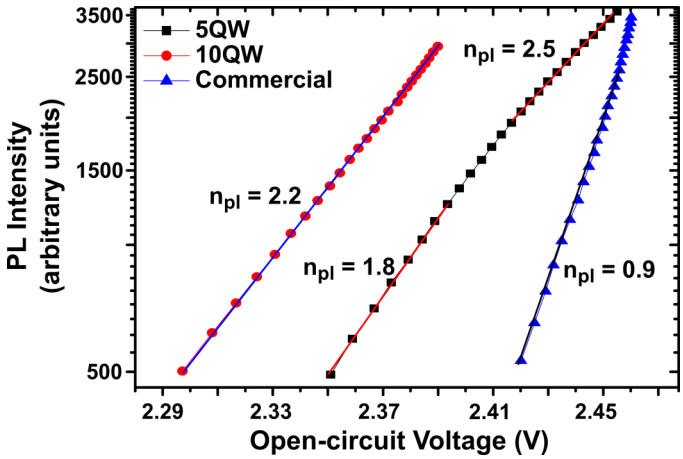

FIG. 10. Semi-log plots of short circuit photoluminescence versus open-circuit voltage for the three samples.

TABLE I. Measured ideality factors from electrical measurements at 300 K and 400 K, from radiative current measurements, from photovoltaic measurements and from photoluminescence.

Sample	n_{elec} (300 K)	n_{elec} (400 K)	n_{light}	n_{pv}	n_{pl}
5QW	3.3	2.6	1.5	2.1 → 2.9	1.8 → 2.5
10QW	3.6	2.8	1.6	2.7	2.2
Commercial	2.1	2.2	1.1	1.0	0.9

The ideality extracted from the J-V measurements are consistently higher than those extracted from the optical measurements. This reflects the contribution of carrier transport outside the intrinsic region of the diode. The J-V measurement is also limited by the resistance of the small area diodes. The optical measurements also involve carrier transport and redistribution in order to establish the forward voltage.

The 5QW sample shows distinctive piezoelectric effects in the red-shifting of the EL with increased bias. It also shows a distinct break in its photovoltage characteristics around 2.4 V which is indicative of relatively reduced radiative recombination above this voltage. One possibility for this change is that the radiative recombination rate is being reduced due to increased field across the wells and a limitation on the radiative recombination through the band-tail states. A second possibility is that part of the measured voltage in the 5QW sample is being dropped across either the finite p/n doping or across each QW/QB pair which is termed QFL loss in reference.[16] This is larger for the hole QFL due to their lower mobility and for QWs on the p-side of the junction. While such the voltage drop should also be present in the 10QW we do not measure strong piezoelectric properties in that sample which could be due to reduced interface charge on the QWs on the p-side of the junction associated with the accumulation of strain in that structure.

V. CONCLUSIONS

We have investigated the effect of a change in the thickness of the QB from 4 nm to 6.6 nm in the active region of InGaN/GaN LEDs when the QW thickness is 1.5 nm. This seemingly small change leads to significant differences in the carrier transport and light emission characteristics of the devices. The differences were compared with a reference LED material which shows different behavior again.

The 10QW sample draws more current at low voltage which we ascribe to trap-assisted tunneling of holes associated with the low-temperature grown barriers and the fact that the barriers themselves are thin. These traps assist in carriers entering the quantum well at low voltages resulting in the ideality >1 for light emission and consistently being the highest among the three samples

measured. The thin barriers also assist in the extraction of carriers in photovoltaic mode. The spectral properties are dominated by bandfilling as opposed to piezoelectric effects suggesting the piezoelectric interface charge is less than for the 5QW sample. The 5QW sample with the thicker barriers shows features in the emission spectra that are associated with a strong piezoelectric field in the quantum well suggesting that the interface charge is large in this case. Partial trapping of carriers is measured in forward bias with carriers entering (current injection) and leaving (photovoltaic mode) the QW region. The light-related idealities for the 5QW and 10QW samples are >1 suggesting non-radiative recombination in the QWs and especially for the 10QW sample. The commercial sample has values for n_{light}, n_{pv} and n_{pl}, each being close to ideal suggesting minimal non-radiative recombination. The higher electrical ideality is due to carrier transport external to the QW region at low voltages and due to resistance at higher voltages. An InGaN underlayer is shown to affect the optically pumped measures of the ideality (n_{pv}, n_{pl}) due to the contribution of additional carriers resulting in extracted idealities even below 1.

ACKNOWLEDGMENTS

The authors would like to thank the funding by the European Communities 7th Framework Programme under Grant 280587 (ALIGHT) and Science Foundation Ireland funded Irish Photonic Integration Centre (IPIC) under grant 12/RC/2276.

[1] Y. Narukawa, M. Ichikawa, D. Sanga, M. Sano, and T. Mukai, J. Phys. D: Appl. Phys. **43**, 354002 (2010).
[2] J. Piprek, Phys. Stat. Solidi **207**(10), 2217 (2010).
[3] A. David and N. F. Gardner, Appl. Phys. Lett. **97**, 193508 (2010).
[4] J. Cho, E. F. Schubert, and J. K. Kim, Las. Phot. Rev. **7**(3), 408 (2013).
[5] M. R. Krames, O. B. Scheking, R. Mueller-Mach, G. O. Mueller, L. Zhou, G. Harbers, and M. G. Craford, J. Disp. Tech. **3**(2), 160 (2007).
[6] B. Galler, M. Sabathil, A. Laubsch, T. Meyer, L. Hoeppel, G. Kraeuter, H. Lugauer, M. Strassburg, M. Peter, A. Biebersdorf, U. Steegmueller, and B. Hahn, Phys. Status Solidi C **8**(7-8), 2369 (2011).
[7] R. Charash, P. P. Maaskant, L. Lewis, C. McAleese, M. J. Kappers, C. J. Humphreys, and B. Corbett, Appl. Phys. Lett. **95**, 151103 (2009).
[8] O. Ambacher, J. Smart, J. R. Shealy, N. G. Weimann, K. Chu, M. Murphy, W. J. Schaff, L. F. Eastman, R. Dimitrov, L. Wittmer, M. Stutzmann, W. Rieger, and J. Hilseneck, J. Appl. Phys. **85**, 3222 (1999).
[9] V. Fiorentini, F. Bernardini, and O. Ambacher, Appl. Phys. Lett. **80**, 1204 (2002).
[10] G. B. Lin, D. Y. Kim, Q. Shan, J. Cho, E. F. Schubert, H. Shim, C. Sone, and J. K. Kim, IEEE Photonics Journal **5**(4), 1600207 (2013).
[11] M. J. Wallace, P. R. Edwards, M. J. Kappers, M. A. Hopkins, F. Oehler, S. Sivaraya, R. A. Oliver, C. J. Humphreys, D. W. E. Allsopp, and R. W. Martin, J. Appl. Phys. **117**, 115705 (2015).
[12] G.K. Reeves, Solid-State Electron. **23**, 487 (1980).
[13] L. Lewis, P. P. Maaskant, and B. Corbett, Semicond. Sci. Technol. **21**, 1738 (2006).
[14] T. E. Sale, J. Woodhead, G. J. Rees, R. Grey, J. P. R. David, A. S. Pabla, P. J. Rodriguez-Gíronés, P. N. Robson, R. A. Hogg, and M. S. Skolnick, J. Appl. Phys. **76**, 5447 (1994).
[15] M. Leroux, N. Grandjean, J. Massies, B. Gil, P. Lefebvre, and P. Bigenwald, Phys. Rev. B **60**, 1496 (1999).
[16] P. Kivisaari, J. Oksanen, and J. Tulkki, J. Appl. Phys. **111**, 103120 (2012).
[17] T. Akasaka, H. Gotoh, T. Saito, and T. Makimoto, Appl. Phys. Lett. **85**, 3089 (2004).
[18] M. A. Reshchikov, D. O. Demchenko, A. Usikov, H. Helava, and Yu. Makarov, Phys. Rev. B **90**, 235203 (2014).
[19] D. Zhu, J. Xu, A.N. Noemaun, J.K. Kim, E.F. Schubert, M.H. Crawford, and D.D. Koleske, Appl. Phys. Lett. **94**, 081113 (2009).
[20] M.A. der Maur, B. Galler, I. Pietzonka, M. Strassburg, H. Lugauer, and A. Di Carlo, Appl. Phys. Lett. **105**, 133504 (2014).
[21] C. L. Reynolds, Jr. and A, Patel, J. Appl. Phys. **103**, 086102 (2008).
[22] X. A. Cao, E. B. Stokes, P. M. Sandvik, S. F. LeBoeuf, J. Kretchmer, and D. Walker, IEEE Elec. Dev. **23**, 535 (2002).
[23] Z. Hu, K. Nomoto, B. Song, M. Zhu, M. Qi, M. Pan, X. Gao, V. Protasenko, D. Jena, and H. G. Xing, Appl. Phys. Lett. **107**, 243501 (2015).
[24] M. Binder, B. Galler, M. Furitsch, J. Off, J. Wagner, R. Zeisel, and S. Katz, Appl. Phys. Lett. **103**, 221110 (2013).
[25] J. M. Lee and S. B. Kim, IEEE Trans. Elec. Dev. **58**, 3053 (2011).
[26] D. S. Meyaard, J. Cho, E. F. Schubert, S. H. Han, M. H. Kim, and C. Sone, Appl. Phys. Lett. **103**, 121103 (2013).
[27] J. J. Wierer, Jr., D. D. Koleske, and S. R. Lee, Appl. Phys. Lett. **100**, 111119 (2012).
[28] J. R. Lang, N. G. Young, R. M. Farrell, Y.-R. Wu, and J. S. Speck, Appl. Phys. Lett. **101**, 181105 (2012).
[29] H. Masui, S. Nakamura, and S. P. DenBaars, Appl. Phys. Lett. **96**, 073509 (2010).
[30] See supplementary material at http://dx.doi.org/10.1063/1.4959100 for details about yellow band emission and correspondences between the photocurrent and the increase in light emission.